Canadian Conference - Pacific Conference on Earthquake Engineering 2023
Vancouver, British Columbia
June 25th – June 30th, 2023

Experimental Investigation of Portal Frames of Selective Pallet Steel Storage Racks under Cyclic Loads

Radin Md Mahirul Hoque[1*], Peng Zhang [1], M. Shahria Alam [1], Robert Tremblay[2]
[1] The University of British Columbia, Kelowna, BC, Canada
[2] Polytechnique Montreal, Montreal, Quebec, Canada
*mahir10ce@gmail.com (Corresponding Author)

ABSTRACT

This study investigated the structural performance of selective pallet steel storage racks against earthquakes through experimentally testing single-level, one bay portal frames under cyclic loads. The study evaluated the lateral load-displacement response of the portal frames, the influences of beam-to-column connections on the responses of the portal frames, energy dissipations and stiffness degradation during the cyclic loading. The portal frame exhibited P-Δ effects and nearly symmetrical behavior in terms of the moment rotation of the connector for cyclic loading. The study found that beam-column with teardrop connections had a significant influence in terms of energy dissipation, viscous damping ratio, and secant stiffness on the moment-rotation hysteresis behavior of the joint. The energy dissipation increased as the development of the plastic deformation in the connector, and the stiffness degradation resulted in reduced pinching effects in the responses of connectors The paper also discusses numerical modeling of the portal frame test and validation using OpenSees software, concluding that the model is suitable for further analysis purposes in simulating the earthquake responses of the joint of the rack clad structure.

Keywords: Selective pallet steel storage racks, portal frame tests, beam-to-column joints, numerical simulations

INTRODUCTION:

Steel storage racks are widely used in warehouses and distribution centers to store and handle materials. These racks are subject to various types of loads, including static and seismic loads. Seismic loads, in particular, pose a significant challenge to the design and performance of steel storage racks due to the potential for damage or collapse during earthquakes. The performance of steel storage racks under earthquakes is largely governed by beam-to-column connections. The beam-to-column connections should be able to withstand the lateral forces induced by earthquakes while maintaining the integrity and stiffness of the connection. The beam-to-column connection design should also ensure that deformations are limited to prevent damage to the racks and the stored materials. Researchers in the past investigated the feasibility of utilizing the displacement-based design approach in the seismic design of selective pallet storage racks in the down-aisle direction [1-3]. The acknowledgment of the potential threat associated with seismic loading-induced failure of rack storage systems has led to recommendations for seismic provisions to be incorporated into the design code of such systems. The FEMA 460 [1] has introduced a displacement-based evaluation procedure for steel storage racks. This approach estimates the structure stiffness via the secant stiffnesses of beam-to-upright connectors and base plates-to-floor connection obtained from cyclic tests. The displacement-based method is an acceptable option for the seismic design of steel storage racks instead of the force-based method, as stated in the RMI Specification [2]. The Canadian design standard of CSA S16 [3] has incorporated a displacement-based approach for the seismic design of steel storage racks. However, insufficient experimental data and numerical validation of the different components of the rack clad structures are preventing the application of the displacement-based design method [3].

Despite the importance of beam-to-upright connections in the seismic performance of steel storage racks, there is limited experimental data on their behavior under seismic loading. A thorough examination of the beam-upright connection, outlining the techniques used to ascertain its properties and discussing the results of parametric studies are discussed by [4]. In the past, there have been a limited number of numerical studies on the steel beam-column joint for cyclic loading [8-13] and only a few experimental studies have focused on the joint connection of rack-clad building (RCB) [14-16]. Previously, the portal frame test was carried out to explore various aspects of the beam upright joint. How the response is affected by viscous damping is studied in [15] . The performance of Bolted moment connections and tab connectors used in the portal beam to upright connections for drive-in and drive-through steel storage racks was analyzed in [16]. The seismic impact of steel storage racks while taking into account changes in the dead load was investigated in [17].

The study investigated the behavior of the connections under different levels of seismic loading and evaluate their performance based on deformation, strength, and energy dissipation characteristics using the portal frame test. This research aimed to establish a robust numerical model of a pallet steel storage rack for seismic simulations in the future.

TEST PROGRAM:

Structural components:

In this study, one type of portal frame was investigated. Figure 1 illustrates the cross-sections of the beam, upright and the profile of beam-to-column teardrop connector with an extended leg.

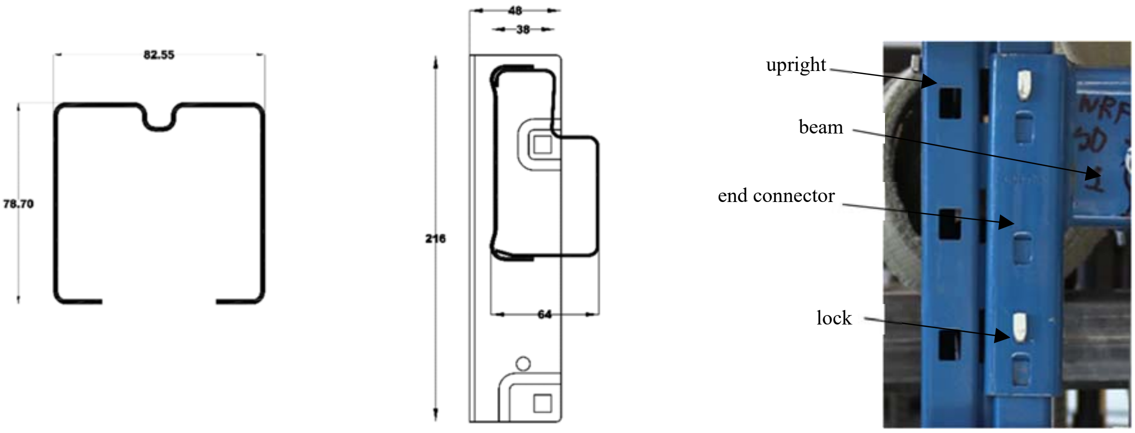

(a) *(b)* *(c)*

Figure 1: geometric cross-section and shape of the beam, uprights, and end connectors. (a) upright cross-section (b) beam cross-section (c) the profile of beam-to-column connector, (all dimensions are in mm).

Test setup:

The portal frame tests were conducted at the Structural Engineering Laboratory of the University of British Columbia following the RMI code[2]. Figure 2 shows a single-level, one bay portal frame test setup in which the beams, columns, and braced were thin-walled, cold-formed steel members. The base of the portal frame, as depicted in Figure 1, consists of a hinge support comprising two 12.7 mm thick steel plates and a shaft located at the center of the upright. The hinge support of the portal frame consists of an upper plate connected to the base plate welded to the upright, and the bottom plate was bolted to a 31.75 mm thick steel plate that was bolted to the strong floor. The frame has a span of 1066.8 mm in the cross-aisle direction and a span of 2515 mm between the center lines of the uprights in the down-aisle direction. The height between the base plate and the top of the beam was consistent at 673 mm for all specimens in the test. Two wooden pallets with a width of 1016 mm and a length of 1219.2 mm were used to bear two concrete blocks representing the dead load in the experiment. The weight of the wooden pallets was included in the total dead load, which amounted to 18.28 kN. To prevent damage to the beam upright connection, the actuator applied displacement through a loading beam, which was attached to an HSS loading beam. The HSS beam was connected to the beam at a distance of $d/3$ from the upright, where d is the clear distance between the upright. By using the HSS loading beam, the lateral force was evenly distributed to the four corners of the frame, rather than applying the lateral force directly to the beam upright.

Instrumentation:

The instruments used in the experiment consisted of Linear Variable Differential Transformers (LVDTs), string pots, and a data acquisition system. Two LVDTs were used for each beam-to-column joint to measure the rotations. One was positioned above the joint while the other was placed below it. Figure 3 illustrates the arrangement of LVDTs for a beam-to-column joint. To prevent the bending of the LVDTs during the test, both ends of the LVDTs were connected with a pinned connection. The LVDTs' supports were screwed to the upright to ensure that they did not move during the test. Four string pots were used to measure the lateral displacements of the four corners of the frame, and the actuator also provided the lateral displacement value. The readings obtained from both the string pots and the actuator were found to be identical

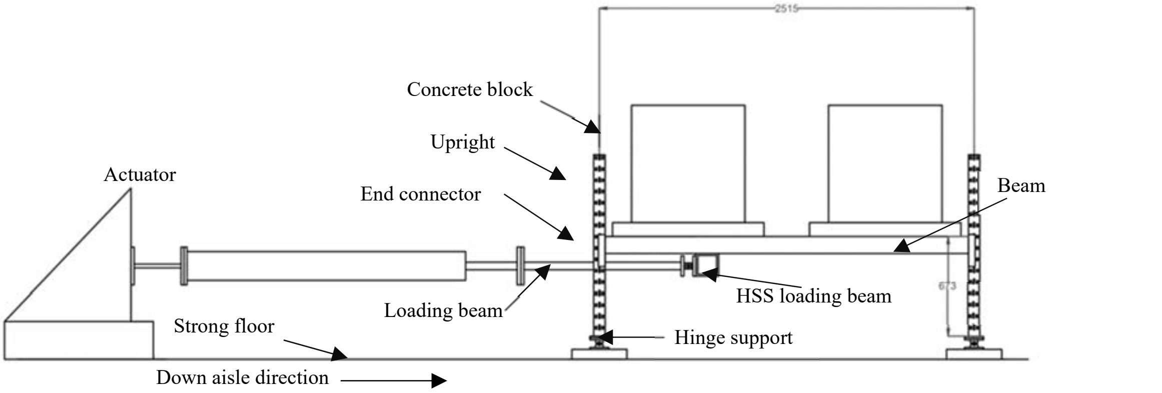

figure 2: Schematic diagram of the portal frame test

Figure 3: Instrumentation of the portal frame test.

Loading protocols:

The cyclic test of the portal frame was a displacement-controlled test. Since there was no loading protocol available for the cyclic test of the portal frame, loading protocols were developed specifically for the portal frame test. A 2D finite element model of the portal frame was created in SAP2000 to develop loading protocols. The model used the geometric properties of the upright, beam, and end connector, and a rotational linear link element was employed as the joint between the beam and column. The stiffness of the link was estimated from a literature review [15-16]. The purpose of this preliminary finite element model was to predict the drift for a specific rotation of the beam-to-column joint. According to the FE model, the difference between the drift ratio and rotation of the connectors was almost negligible, which can be explained by equation (1). This equation is taken from[18]. The equation shows a relationship between the rotation of the end connector and the drift of the portal frame test.

$$\theta_c = \frac{\Delta_{avg}}{H} - F\left(\frac{H^2}{12EI_c} + \frac{HL}{24EI_b}\right) \quad \text{........} \quad (1)$$

Here,
θ_c= the rotation of the beam-to-column joint
F= the total applied lateral load
H= distance between the center of the beam and the shaft of the beam
Δ_{avg} = the average lateral displacement of the four beam-to-column joints
L= the distance between the centerlines of the two columns in the down-aisle direction

From the FE analysis using the loading protocol for the beam upright joint test in CSA S16[3], a suitable loading protocol for the portal frame test was developed.

In the initial test, the CSA S16 [3] loading protocol was used. The results of the first test were used to improve the accuracy of the SAP model by incorporating the rotational stiffness properties of the beam-upright joint. Based on this improved model, two additional loading protocols were developed.

Selecting adequate ground motions is critical for developing loading protocols. The chosen ground motions should reflect the seismic risk in the region where the structures are planned to be built [19]. So, a Suite of 22 ground motion records for a Vs = 360 m/s site in Vancouver, BC, Canada, was selected to develop the loading protocols. Selection and scaling per the procedure given in the guidelines of Commentary I of NBC 2020 [20]. Eleven ground motion records are from Shallow and In slabs earthquakes, and the other 11 ground motion records are from Subduct interface earthquakes. Nonlinear time history analysis was performed in SAP2000 using these ground motion records. From the FE analysis, the displacement time-history responses with varying amplitude need to be converted into constant amplitude cycles to create equivalent blocks. To accomplish this task, a rain flow counting algorithm was used for cycle counting. Three factors: cumulative damage model, energy loss, and cumulative distribution function were considered to develop the loading protocol from the rain flow counting algorithm data. The three loading protocols are shown in Figure 4. The loading protocols developed from CSA S16 [3], shallow earthquakes, subduction interface earthquakes are termed as CY1, CY2, and CY3 loading protocols, respectively.

A 50 kN capacity actuator was used in the test, and the displacement load was applied at the rate of 15 mm/min. The out-of-plane movement of the portal frame was restrained by providing lateral support to the portal frame.

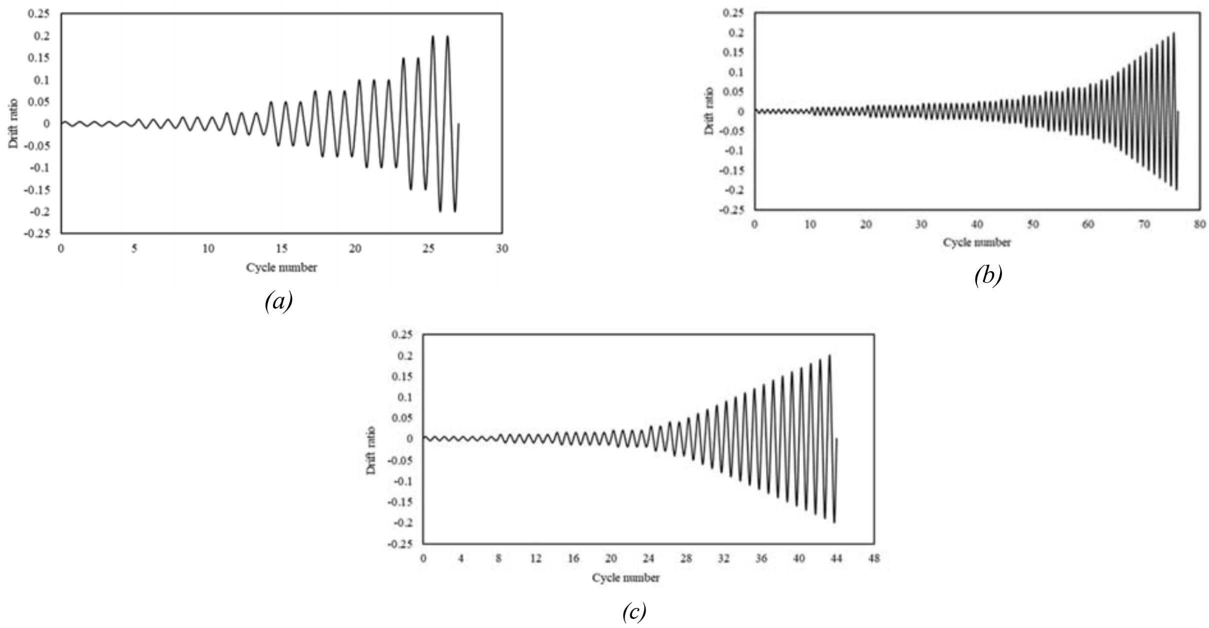

Figure 4: Loading protocols for the portal frame test (a) CY1 loading (b) CY2 loading (c) CY3 loading.

EXPERIMENTAL RESULTS:

Figure 5 shows the responses of the portal frame under the CY2 loading protocol. Figure 5(a) shows lateral load-displacement, and Figure 5(b) shows the moment-rotation relationship. In Figure 5(a), the lateral load is the overall lateral load applied to the frame, and the lateral displacement is the average displacement of the four beam-to-column corners. In Figure 5(b), the rotation refers to the rotation of the joint of the beam-upright connection, and the moment is the joint moment. The load-deformation response in a hysteretic loop is nearly symmetrical under positive and negative loads. The portal frame specimen comprises a cold-formed beam, and an upright, and semi-rigid end connector, resulting in a flexible structure that exhibits noticeable P-delta effects in Figure 5. When calculating the beam-to-column joint moment, the P-delta effect was taken into account. The equation for calculating the moment is shown in equation (2).

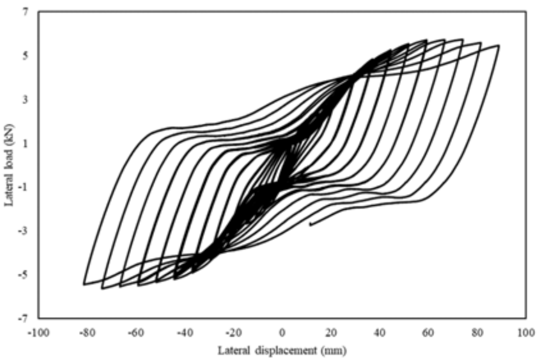

(a)

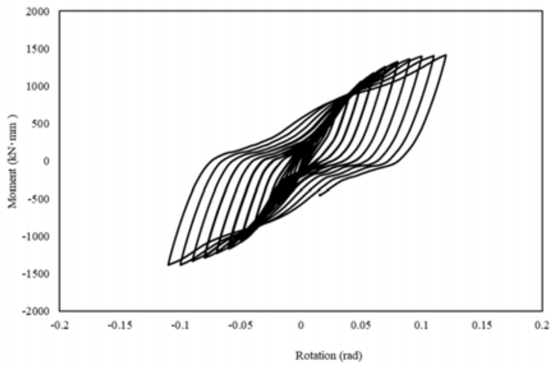

(b)

Figure 5: (a) lateral force-displacement relationship of the portal frame test; (b) moment-rotation relationship of the connection of the beam-upright joint in CY2 loading protocol test.

$$M_c = (F * H + W * \Delta_{avg})/4 \quad ...(2)$$

Here, *W* is total dead load. The rotation of the beam-to-column joint was calculated based on the two readings from the LVDTs that were attached to that joint (see Figure 3). The equation for calculating the rotation is given in Eq. (3).

$$\theta_c = (d1 - d2)/h \quad ..(3)$$

Here,
θ_c = the rotation of the beam-to-column joint
d1, d2 = displacements read from the LVDTs
h = the distance between the two LVDTs.

To evaluate the accuracy of the LVDTs, the calculated rotations based on the LVDT results were compared with the rotations calculated using Eq. (1). The two results were found to be the same.

It was observed that the beam-to-column joints had a significant influence to the response of the portal frame, as demonstrated by the similarities observed between Figure 5(a) and Figure 5(b). The hysteresis response of the moment-rotation has a minor pinching. The end connector of the beam became loose from the upright due to various mechanisms of yielding and buckling, which results in a pinching effect in the hysteresis response. As the number of loading cycles increases, the pinching effect became less significant (figure 6c & 6d). Although the end connector began to buckle, the holes on the columns was not damaged as much as the beam-end connector (figure 6a & 6b). Therefore, the pinching effect was less visible at higher loading. Figure 6a and figure 6b show that the damaged holes on the column were little damaged compared to undamaged hole , while end connector was deformed significantly.

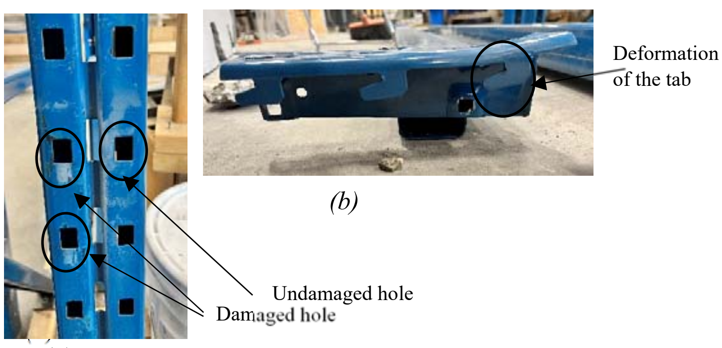

(a) *(b)*

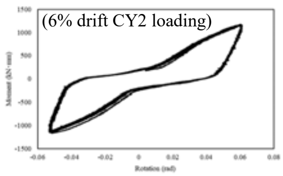

(c)

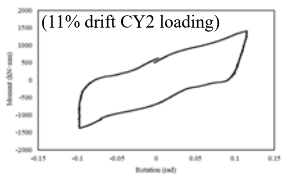

(d)

Figure 6: (a) deformation of the upright's hole; (b) deformation of the end connector;(c) moment-rotation response at 6% drift under CY2 loading protocol; (d) moment-rotation response at 11% drift under CY2 loading protocol.

This means that the hole on the upright was the first to sustain damage, leading to the appearance of the pinching effect. However, as the load was further increased, the end connector began to yield and buckle, while the condition of the holes in the upright remained intact. So, the connection between the upright and the end connector became locked as the load increased, resulting in a reduced pinching effect observed in the response (figure 6c and 6d). Before the lateral load began to decrease, the welded joint connecting the beam and the end connector started to tear. Thus, the failure criteria for the portal frame was the tearing of the welded joint between the beam and the end connector (figure 7).

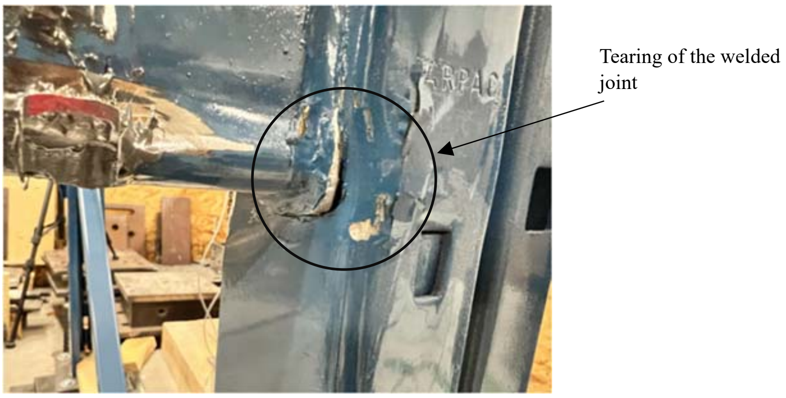

Figure 7: tearing of the welded joint between the beam and the end connector in CY3 loading protocol test.

Energy dissipation:

For assessing the seismic performance, it is important to evaluate a structure's capability to absorb energy under cyclic loads. The areas enclosed by the hysteresis loops were calculated. For each beam-to-column joint, cumulative energies were calculated using experimental data (Figure 5(b)). Be noted that the total energy consists of the positive energy in the first quadrant and the negative energy in the third quadrant. The relationship between total energy, positive energy, negative energy dissipation, and drift of the portal frame under different cyclic loadings are presented in Figure (8). During the elastic stage, the beam-to-column joints exhibited little energy dissipation, and the energy dissipation increased as the plastic deformation of the connector developed. The peak energy dissipation took place prior to the tabs deformed and the cracking of the welding area between the beam and beam end connector.

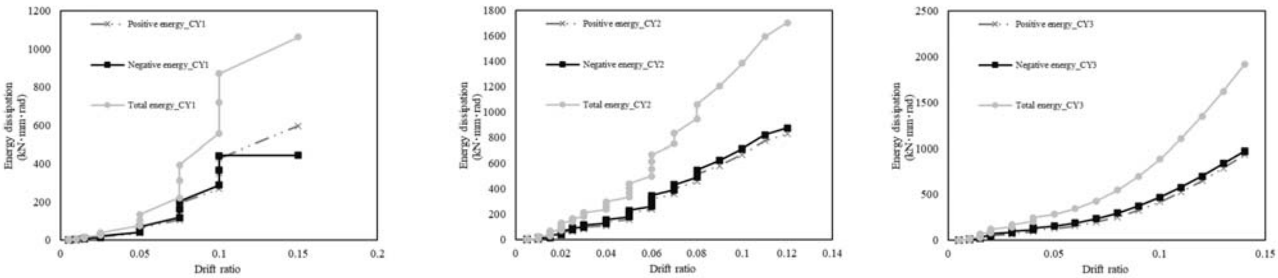

(a) *(b)* *(c)*

Figure 8: Energy dissipation of the beam end connector for three loading protocols test: (a) energy dissipation vs drift ratio for CY1 loading; (b) energy dissipation vs drift ratio for CY2 loading; (c) energy dissipation vs drift ratio for CY3 loading.

Equivalent viscous damping

The equivalent viscous damping ratio measures the energy dissipation capacity of a structure, and it is commonly used to represent the damping properties of a structural system in seismic analysis. For the beam-to-column joints of steel storage racks, the equivalent viscous damping ratio can be used to estimate their energy dissipation capacities. The equivalent viscous damping ratio is important for predicting the dynamic response of the structure during a seismic event. The equivalent viscous damping ratio can be calculated from Eq. (4) derived from [21].

$$\xi = \frac{1}{4\pi}\frac{E_{total}}{E_{els}} \text{ ...(4)}$$

E_{total} refers to the total energy stored in a beam-to-column joint during a cyclic load, which is represented by the area enclosed within a hysteresis loop. Elastic strain energy (E_{el}), on the other hand, is the portion of the strain energy that can be recovered, and it is calculated for each hysteresis loop by determining the area of the triangle formed by the origin, the point of maximum load and its corresponding displacement, and the horizontal axis, in both positive and negative directions. The graphs shown in Figure (9) illustrate the variations of equivalent viscous damping ratios (under positive and negative loads) against the drift of the portal frame. The figures show that the patterns of the equivalent viscous damping ratios under positive and negative loads are nearly the same under each loading protocol.

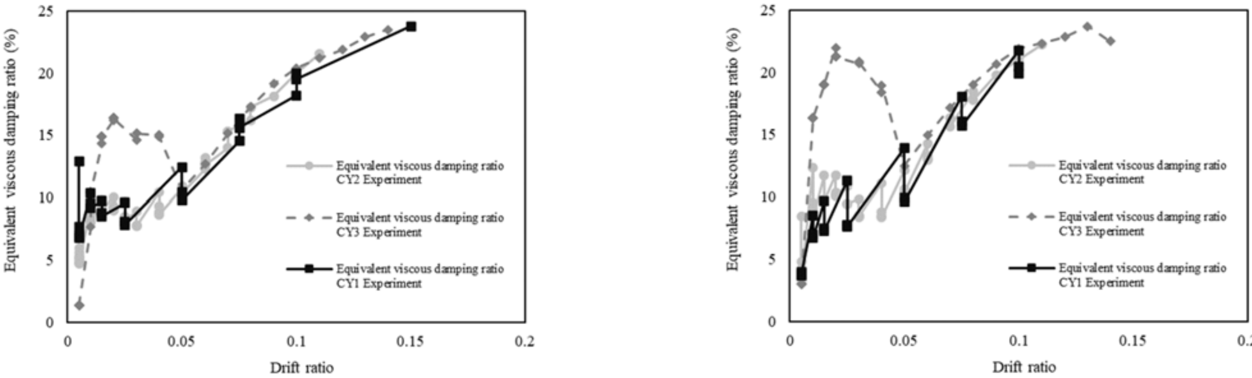

(a) *(b)*

Figure 9 equivalent viscous damping ratio for the three tests: (a) positive equivalent viscous damping ratio; (b) negative equivalent viscous damping ratio.

Stiffness degradation:

In the context of the moment-rotation relationship of the connector, the term "positive secant stiffness" refers to stiffness in the first quadrant, while "negative secant stiffness" refers to stiffness in the third quadrant. Figure 10 presents the secant stiffness degradation with respect to drift ratio. As the lateral displacement of the portal frame is increased, the secant stiffnesses are decreased. In the case of positive loading, the secant stiffnesses at low drift ratio range are scattered. Initially, the connector may require some initial movement to properly lock with the upright's holes, causing a delay in engagement. AS the lateral displacement increases, the engagement between the beam-end connectors and columns improves. It can be observed from Figure (10) that as the increased drift ratios, the curves for the different loading protocols gradually merge together. Initial slippage between the beam-end connectors and columns might be one of the reasons for the scattered secant stiffnesses exhibited at the low range of the drift ratio.

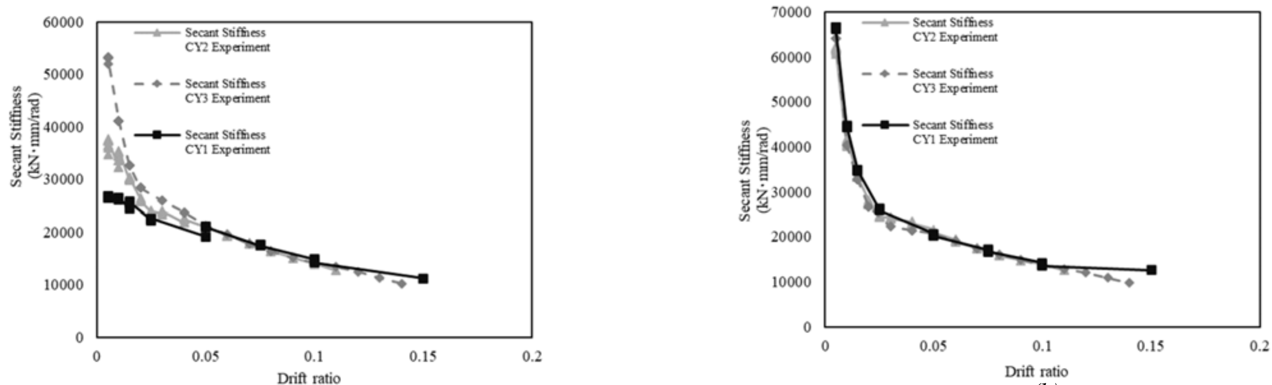

(a) *(b)*

Figure 10: Secant stiffness degradation of the connector for the three tests: (a) positive secant stiffness degradation with respect to drift ratio;(b) negative secant stiffness degradation with respect to drift ratio.

NUMERICAL MODELING:

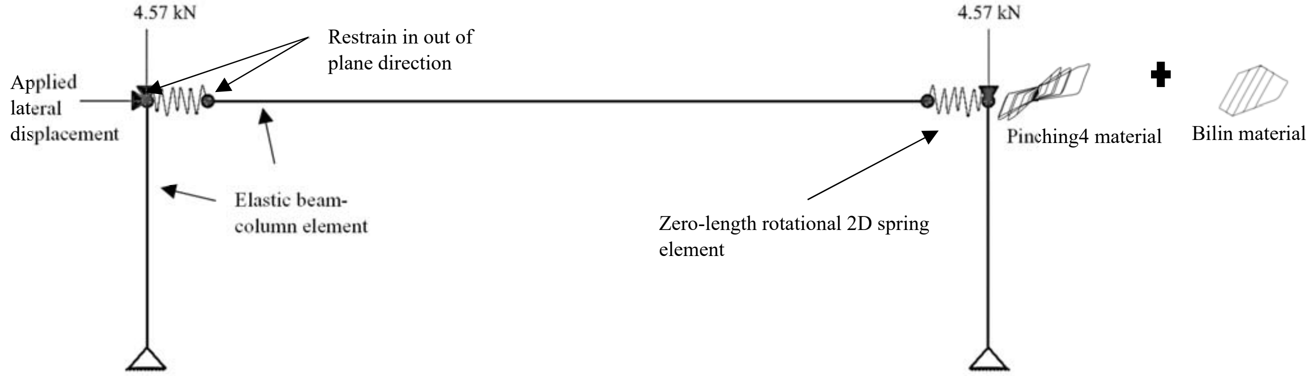

Figure 11: 2D finite element model of portal frame in Opensees.

In figure 11, the schematic diagram of the FE model of the portal frame is shown. For finite element simulations, Opensees [22] was used. OpenSees is a software for simulating structural and geotechnical systems under earthquakes. Two types of elements were used. The elastic beam-column element was used to model the beam and column, and they were drawn along the centerlines of the beam and columns. The second-order P-Δ effect was considered in the model. The material properties of the beam and column were obtained from material property tests. To describe the nonlinear behaviour of the beam-to-column joints, a zero-length rotational 2D spring was considered in the model. Pinching4 material was used for the 2D spring element. Pinching4 material can capture the pinched load-deformation behavior and demonstrate cycle degradation of strength and stiffness. In Figure (5), it can be seen that when the portal frame experienced large lateral displacement, the pinching of the hysteresis loop is insignificant. To capture this behavior in the model, a Bilin material was used in the rotational 2D spring in parallel with the Pinching4 material. Then the 2D spring element was calibrated against the CY1 loading test results. The dead load for each corner of the portal frame specimen, 4.57 kN was assigned at the top of the upright.

Validation of the numerical model:

The 2D FE spring model of the portal frame was calibrated against the test results of the CY1 loading protocol. In Figure 12, the moment-rotation response of the beam-to-column joint obtained from the experiment is compared with the numerical result. The difference between the total energy dissipations obtained from the experiment and the FE result is 10%. Using this FE model, the responses of the portal frame under the CY2 and CY3 loading protocols were predicted. The predicted results were compared with the experimental results. The comparison shows good agreement between the FE and experimental results. The numerical results obtained from the CY2 and CY3 loading protocols differed from the experimental results by the maximum of 6% and 7%, respectively.

Figure 13 presents a comparison between the experimental and FE results in terms of secant stiffness degradation, energy dissipation, and equivalent viscous damping ratio. The FE results agreed well with the experimental results, so the FE model can be used in future for seismic analysis of the frame for different stories.

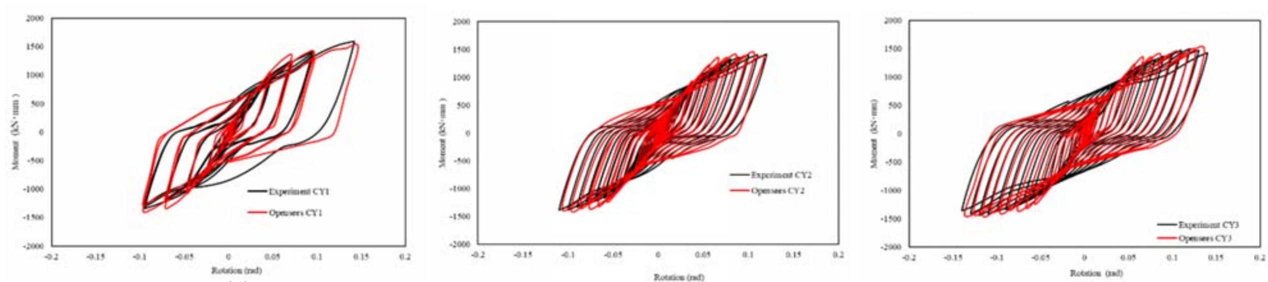

(a) (b) (c)

Figure 12: Comparison of the connectors' moment-rotation responses obtained from the experiments and numerical simulations: (a) Moment vs rotation response for CY1 loading; (b) Moment vs rotation response for CY2 loading; (c) Moment vs rotation response for CY3 loading.

(a) (b) (c)

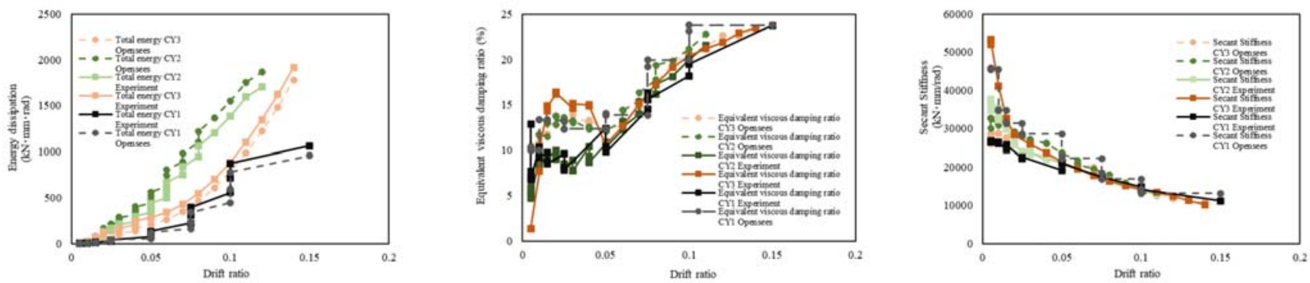

(a) *(b)* *(c)*

Figure 13: Comparison between the experimental data and the FE model results for three different loading protocols: (a) energy dissipation vs drift ratio for three loadings; (b) equivalent viscous damping ratio vs drift ratio for three loadings; (c) secant stiffness vs drift ratio for three loadings.

CONCLUSION:

A portal frame test program was conducted to investigate the behavior of a selective pallet steel storage rack under seismic loading conditions. Three different cyclic loading protocols were developed for the tests.

The load-lateral displacement responses of the portal frames were captured, and the energy dissipation and stiffness degradation of the beam-to-column joints with the loading were determined.

This paper also discusses the energy dissipation of the structure during cyclic loadings. It was observed that the energy dissipation capacity increased as plastic deformation developed and reached its peak before the tabs became deformed and the welding area between the beam and beam end connector experienced cracking. The equivalent viscous damping ratio was calculated to estimate the energy dissipation capacity of the joint, which is important for predicting the dynamic response of the structure during a seismic event. The max equivalent viscous damping ratio was 22% at 15% drift.

The stiffness degradation of the portal frame was evaluated. At first, the secant degradation value differ but with increased load, the value of stiffness was identical. At the 15% drift the secant stiffness value was around 10000 kN.mm/rad.

It was observed that the structure exhibited pinching effects due to the yielding and buckling of the end connector. The pinching effect became less significant as the load increased, resulting in a reduced pinching effect observed in the response. The failure criteria for the specimen was the tearing of the welded joint between the beam and the end connector.

The numerical modeling and validation of a portal frame using the OpenSees software were discussed. To validate the numerical model, the FE model of the portal frame was calibrated using the first test data, and the moment rotation response of the beam-upright joint was compared with the experimental result. The comparison showed good agreement between the FE model and the experimental result. Overall, based on the comparison between the FE model and experimental data for various behavior parameters, it can be concluded that the FE model is suitable for further analysis purposes.

This study only examined one specimen under cyclic loading. To gain a more comprehensive understanding of the structural behavior, more specimens can be studied and compared. A parametric study can also be conducted to determine the factors that influence the structural response under seismic loads. Additionally, the established FE model can be utilized for further seismic analysis.

ACKNOWLEDGEMENT

The financial contribution of the Natural Sciences and Engineering Research Council (NSERC) of Canada through Alliance Grant was crucial to conduct this study and has been gratefully acknowledged.

REFERENCES

[1] FEMA-460, “Seismic Considerations for Steel Storage Racks,” *Build. Seism. Saf. Counc. Natl. Inst. Build. Sci.*, no. September, p. 160, 2005.

[2] RMI, “ANSI MH16.1: Specification for the Design, Testing and Utilization of Industrial Steel Storage Racks,” vol. 2012, p. 48, 2012.

[3] Canadian Institute of Steel Construction, “Handbook of Steel Construction,” *Handb. Steel Constr.*, p. 1092, 2017.

[4] R. M. M. Hoque, P. Zhang, M. S. Alam, and R. Tremblay, “Investigation on Teardrop Connection of Rack Clad

Building," *Int. Conf. Civil, Struct. Transp. Eng.*, no. 161, pp. 1–9, 2021, doi: 10.11159/iccste21.161.

[5] A. M. S. Freitas, M. S. R. Freitas, and F. T. Souza, "Analysis of steel storage rack columns," *J. Constr. Steel Res.*, vol. 61, no. 8, pp. 1135–1146, 2005, doi: 10.1016/j.jcsr.2005.02.004.

[6] K. M. Bajoria and R. S. Talikoti, "Determination of flexibility of beam-to-column connectors used in thin walled cold-formed steel pallet racking systems," *Thin-Walled Struct.*, vol. 44, no. 3, pp. 372–380, 2006, doi: 10.1016/j.tws.2006.01.007.

[7] A. L. Y. Ng, R. G. Beale, and M. H. R. Godley, "Methods of restraining progressive collapse in rack structures," *Eng. Struct.*, vol. 31, no. 7, pp. 1460–1468, 2009, doi: 10.1016/j.engstruct.2009.02.029.

[8] K. M. Bajoria, K. K. Sangle, and R. S. Talicotti, "Modal analysis of cold-formed pallet rack structures with semi-rigid connections," *J. Constr. Steel Res.*, vol. 66, no. 3, pp. 428–441, 2010, doi: 10.1016/j.jcsr.2009.10.005.

[9] A. Crisan, V. Ungureanu, and D. Dubina, "Behaviour of cold-formed steel perforated sections in compression. Part 1 - Experimental investigations," *Thin-Walled Struct.*, vol. 61, pp. 86–96, 2012, doi: 10.1016/j.tws.2012.07.016.

[10] Đ. Jovanović, D. Žarković, V. Vukobratović, and Z. Brujić, "Hysteresis model for beam-to-column connections of steel storage racks," *Thin-Walled Struct.*, vol. 142, no. April, pp. 189–204, 2019, doi: 10.1016/j.tws.2019.04.056.

[11] Emily Jacobsen, "Seismic Behaviour, Numerical Modelling and Displacement-Based Design of Steel Storage Rack Structures for Canadian Applications," ÉCOLE POLYTECHNIQUE DE MONTRÉAL, 2017.

[12] C. Bernuzzi, N. Draskovic, and M. Simoncelli, "European and United States approaches for steel storage pallet rack design. Part 2: Practical applications," *Thin-Walled Struct.*, vol. 97, pp. 321–341, 2015, doi: 10.1016/j.tws.2015.08.011.

[13] C. Bernuzzi, A. Gobetti, G. Gabbianelli, and M. Simoncelli, "Unbraced pallet rack design in accordance with European practice-Part 2: Essential verification checks," *Thin-Walled Struct.*, vol. 86, pp. 208–229, 2015, doi: 10.1016/j.tws.2014.06.014.

[14] F. Gusella, G. Lavacchini, and M. Orlando, "Monotonic and cyclic tests on beam-column joints of industrial pallet racks," *J. Constr. Steel Res.*, vol. 140, pp. 92–107, 2018, doi: 10.1016/j.jcsr.2017.10.021.

[15] E. Jacobsen and R. Tremblay, "Shake-table testing and numerical modelling of inelastic seismic response of semi-rigid cold-formed rack moment frames," *Thin-Walled Struct.*, vol. 119, no. June, pp. 190–210, 2017, doi: 10.1016/j.tws.2017.05.024.

[16] B. P. Gilbert and K. J. R. Rasmussen, "Bolted moment connections in drive-in and drive-through steel storage racks," *J. Constr. Steel Res.*, vol. 66, no. 6, pp. 755–766, 2010, doi: 10.1016/j.jcsr.2010.01.013.

[17] N. ASAWASONGKRAM, P. Chomchuen, and P. Premthamkorn, "Seismic Performance Evaluation of Steel Storage Racks Using Experimental Results of Beam-To-Column Connection," *Second Eur. Conf. Earthq. enginnering Seismol.*, pp. 1–12, 2014, [Online]. Available: http://www.eaee.org/Media/Default/2ECCES/2ecces_eaee/1304.pdf

[18] H. Krawinkler, "Experimental Study on Seismic Behavior of Industrial Storage Racks.," *Proc. - Annu. Public Water Supply Eng. Conf.*, vol. 2, pp. 749–781, 1978.

[19] H. Krawinkler *et al.*, "Development of a Testing Protocol for Woodframe Structures," *CUREE - Caltech Woodframe Proj.*, no. April, pp. 1–76, 2001, [Online]. Available: https://www.curee.org/publications/woodframe/downloads

[20] Canadian Commission on Building and Fire Codes, *National Building Code of Canada: 2020*, vol. 1. 2022.

[21] "Earthq Engng Struct Dyn - 1999 - Pekcan - Fundamental considerations for the design of non-linear viscous dampers.pdf."

[22] "Opensees." [Online]. Available: https://opensees.berkeley.edu/